Hyperspectral Target Detection Using K-Means Clustering Algorithm

Akhilesh S.S
PG Student
Department of ECE
Satyam College of Engineering
E-mail : cutboy.akhileshss@gmail.com

Abstract

This paper introduces a novel classification strategy based on the monogenic scale space for target recognition in Synthetic Aperture Radar (SAR) image. The proposed method exploits monogenic signal theory, a multidimensional generalization of the analytic signal, to capture the characteristics of SAR image, e.g., broad spectral information and simultaneous spatial localization. The components derived from the monogenic signal at different scales are then applied into a recently developed framework, sparse representation-based classification (SRC). Moreover, to deal with the data set, whose target classes are not linearly separable, the classification via kernel combination is proposed, where the multiple components of the monogenic signal are jointly considered into a unifying framework for target recognition.

Keywords: **The monogenic signal, sparse representation, SAR target recognition, composite kernel learning, score-level fusion, monogenic scale-space.**

I. INTRODUCTION

DUE to the capability to produce all-weather, 24-hour a day, high-resolution images with quality quickly approaching that of optical imaging sensors, Synthetic Aperture Radar (SAR) has been used in many fields. Automatic target recognition (ATR) is an essential topic for SAR image interpretation. In the past several decades, SAR conditions (EOC) [1], [2], in which a single operational parameter is significantly different between the images used for training and those for testing. The baseline SAR ATR system comprises three separate stages: detection, discrimination, and classification [3]. The first stage roughly locates the candidate targets in a SAR image by examining the amplitude of the radar signal in each site of the image. The second stage rejects the natural-clutter false alarms with some discriminants (*e.g.*, standard deviation, fractal dimension, and weighted-rank fill ratio [4]), followed by a classifier to reject the culturalclutter false alarms and predict the target type of the remaining detections [5]. This paper mainly focuses on classification.

Carl A. Wiley, a mathematician at Goodyear Aircraft Company in Litchfield Park, Arizona, invented synthetic aperture radar in June 1951 while working on a correlation guidance system for the Atlas ICBM program. In early 1952, Wiley, together with Fred Heisley and Bill Welty, constructed a concept validation system known as DOUSER ("Doppler Unbeamed Search Radar"). During the 1950s and 1960s, Goodyear Aircraft (later Goodyear Aerospace) introduced numerous advancements in SAR technology, many with the help from Don Beckerleg.

Independently of Wiley's work, experimental trials in early 1952 by Sherwin and others at the University of Illinois' Control Systems Laboratory showed results that they pointed out "could provide the basis for radar systems with greatly improved angular resolution" and might even lead to systems capable of focusing at all ranges simultaneously.

In both of those programs, processing of the radar returns was done by electrical-circuit filtering methods. In essence, signal strength in isolated discrete bands of Doppler frequency defined image intensities that were displayed at matching angular positions within proper range locations. When only the central (zero-Doppler band) portion of the return signals was used, the effect was as if only that central

part of the beam existed. That led to the term Doppler Beam Sharpening. Displaying returns from several adjacent non-zero Doppler frequency bands accomplished further "beam-subdividing" (sometimes called "unfocused radar", though it could have been considered "semi-focused"). Wiley's patent, applied for in 1954, still proposed similar processing. The bulkiness of the circuitry then available limited the extent to which those schemes might further improve resolution.

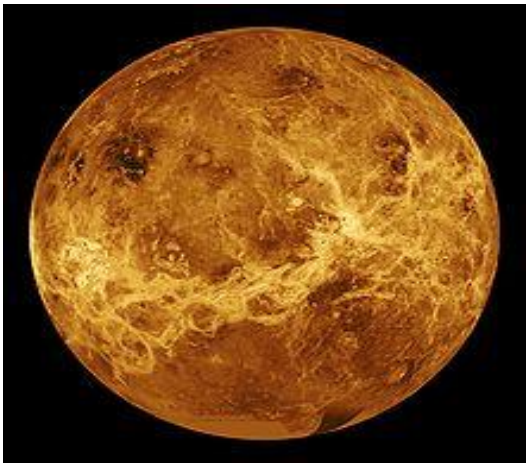

Figure 1.1: The surface of Venus, as imaged by the Magellan probe using SAR

The principle was included in a memorandum[9] authored by Walter Hausz of General Electric that was part of the then-secret report of a 1952 Dept. of Defense summer study conference called TEOTA ("The Eyes of the Army"),[10] which sought to identify new techniques useful for military reconnaissance and technical gathering of intelligence. A follow-on summer program in 1953 at the University of Michigan, called Project Wolverine, identified several of the TEOTA subjects, including Doppler-assisted sub-beam width resolution, as research efforts to be sponsored by the Department of Defense (DoD) at various academic and industrial research laboratories. In that same year, the Illinois group produced a "strip-map" image exhibiting a considerable amount of sub-beamwidth resolution.

In [18], the recognition problem is cast as one of classifying among multiple linear regression models, and addressed by the sparse signal representation. By sparsity constraint (_1-norm minimization), the unique representation can be generated. The
decision is made by evaluating which class of samples could recover the query as accurately as possible. Since SAR images of a given class lie in a manifold, whose dimension is much lower than the actual one [19], the training images can be assumed to be the samples drawn from the manifold. Then, the classification of SAR image is equivalent to finding the manifold that is closest to the query image. According to the point of local linear embedding algorithm [20], linear representation can be provided to any nonlinear manifold if only a small local region is considered. Thus, it is applicable for sparse signal representation to SAR image-based target recognition, as verified in [21]–[25].
Recently, a novel 2D analytic signal named the monogenic signal is presented in [26] and [27]. It has been built around the Riesz transform, a 2D vector-valued extension of Hilbert transform [28]. As a generalization of the analytic signal, the monogenic signal could preserve the properties of analytic signal concerning symmetry, energy, all pass transfer function, as well as the invariance-equivariance property with respect to phase and orientation. Thus, it has been widely studied in the preceding works. In [29] and [30], a 2D monogenic wavelet transform is presented for image analysis. The main advantage of monogenic wavelet transform consists in the capability to offer a geometric representation for gray-scale image through an AM-FM model allowing invariance of coefficients to translations and rotations. In [31], a binary encoding scheme named monogenic binary coding is presented for biometric recognition. The components of the monogenic signal are encoded by various binary pattern schemes, followed by a nearest neighbor classifier to make the decision. In [32], the monogenic signal is used for optical flow estimation, where the displacement is locally computed

by assuming the conservation of the monogenic phase over time. Moreover, the monogenic signal is employed for SAR target recognition in [23] and [24]. To make the algorithm computationally tractable, a monogenic feature descriptor is formed via concatenating the monogenic components. Since various kinds of information are roughly combined, it may result in some information loss. To cover the shortage, this
paper introduces the score-level fusion. Real part, *i* –imaginary part, and *j* -imaginary part of the monogenic signal at various scales are used to generate three different feature descriptors, from which three sparse representation-based classifications can be built. Specifically, the features of training samples are used to build a redundant dictionary to represent the counterpart of the query as a linear combination of them. The unique representations can be generated via sparsity constraint (_1-norm minimization), as similar to [18], [23], and [24]. Then, the results of individual classification are combined by performing score-level fusion [33]. Though the performance can be improved by score-level fusion strategy, it may be not effective if the target classes are not linearly separable. To address the problem, this paper embeds the monogenic features into a high-dimensional Hilbert space induced by a kernel function. Given the nonlinear mappings, the proposed monogenic features can be transformed into the Hilbert spaces, where the query can be linearly represented in terms of the training samples. To jointly consider these features in a unifying system for target recognition, the component-specific Hilbert spaces are combined to form a larger global one by composite kernel learning [34]. Then, the similarity between a pair of samples can be evaluated more accurately. To produce the unique representation, this paper employs linear coding (_2-norm minimization) strategy [35], [36], rather than sparse coding one (_1-norm minimization) [37], [38] to limit the feasible set of the representations. This is because the data separability between different classes has been enhanced in the global Hilbert space, and a linear coding strategy could yield the performance similar to sparse coding method yet with less computational cost. Finally, the inference is reached according to the characteristics of the representation on reconstruction.

The reminder of this paper is organized as follows. Section II briefly reviews the formulation of sparse coding and linear coding in the Hilbert space, as well as the kernel tricks. Section III devotes to the proposed classification via score-level fusion and the one via composite kernel learning. The effectiveness of the proposed methods has been evaluated in Section IV by several experiments on Moving and Stationary Target Acquiration and Recognition (MSTAR) database. Finally, Section V concludes this paper.

2 RELATED WORKS

The proposed method exploits monogenic signal theory a multidimensional generalization of the analytic signal, to capture the characteristics of SAR image, e.g., broad spectral information and simultaneous spatial localization. The feasibility of the proposed method has been successfully verified using Moving and Stationary Target Acquiration and Recognition database. Previously, three individual classifications are formed on the monogenic scale-space, and the results of which are combined by score-level fusion scheme. Though the performance can be improved, it may be not effective if the classes are not linear separable. To address this problem, a popular idea is to cast the samples into the Hilbert space whose dimension is high or even infinite. Then, the similarity between a pair of samples can be estimated in a sufficiently rich feature space (F).Given a nonlinear mapping (·): Rm→F,by which the monogenic features can be cast into the Hilbert space. Inspired by the preceding work where the spatial and spectral information are combined by constructing a family of composite kernels, this paper proposes to combine the information contained in the monogenic signal by composite kernel learning. We first integrate three component-specific Hilbert spaces into a larger global space, in which the similarity between a pair of samples could be evaluated more accurately. Monogenic representation. For any new test sampley,it is represented by three monogenic feature descriptors,χ R(y), χI(y), χJ(y), formed on log-Gabor filters induced monogenic scale-space.

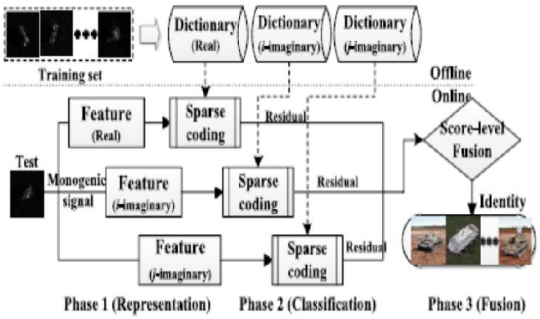

Figure 2.1: The block diagram of classification via score-level fusion. Three classifications are formed by real part, i-imaginary part, and j-imaginary part of the monogenic signal. The results are combined by performing score-level fusion (Bayesian inference).

• ***Kernel combination.***

The monogenic features are embedded into the Hilbert spaces with the non linear mappings. By stacked features or summation kernel, the component-specific Hilbert spaces are combined to forma larger global space.

• Make decision. In the global Hilbert space, the query is represented as a linear combination of training samples.

The flowchart of classification via kernel combination. The monogenic features generated on the monogenic scale-space are embedded into the Hilbert spaces. The component-specific Hilbert spaces are combined to forma larger one, in which linear coding strategy is used to make the decision. coding strategy, and the decision is made according to the characteristics of the representation on reconstruction. Since the first step has been stated previously, the following section will pay more attention to kernel combination. three monogenic features are generated on the monogenic scale-space. To combine the information contained in the monogenic features, this paper joint l considers these features into a unifying framework for target recognition. It is realized by a recently developed earning skill, kernel combination. two schemes are contended. Scheme 1 (Stacked Features):The first scheme refers to forming an augmented feature $\chi c \in Rd$ by stacking the monogenic features χR, χI and χJ to be an single vector, as similar to the preceding work. Then, we cast the resulting augmented feature into the Hilbert space Fc. For any two samples{xp,xq}, if denote by $\varphi c(\cdot)$: $Rd \rightarrow Fc$ the mapping that projects an augmented feature into the Hilbert space Fc, the kernel can be formed

3 IMPLEMENTATION

1) Verify the preliminary performance of the proposed method. Three targets,TG1, TG2,andTG3 are utilized, among whichTG1andTG3have three variants with structural modifications, as illustrated in Fig. 6.The standards (SN_9563 forTG1 and SN_132 forTG3)taken at 17° depression are used to train the algorithm, while the remaining collected at 15° depression are used for testing, i.e., the variants used for testing are not contained in the training set.

2) To assess the performance under different feature spaces, four down-sampling factors ρ =1400,1256,1100,164are tested.

(i) The classification via data fusion significantly outperforms the individual classifications. Under 16D feature space, the recognition rates for MSRC, SUM, and MAP are 0.8368, 0.8429, and 0.8542, compared to 0.6961 for SRCR, 0.7669 for SRCI, 0.8183 for SRCJ. The similar performance can be achieved under the other feature spaces.

(ii) The performance of score-level fusion always exceeds the one of feature-level fusion. Under 16D, 25D,64D, and 100D feature spaces, the recognition rates for MAP are 0.8542, 0.8963, 0.9302, and 0.9487, compared to 0.8368, 0.8932, 0.9179, and 0.9322 for MSRC. It is 1.74%, 0.31%, 1.23%, and 1.65% better than the competitor. The result proves that the combination by concatenating monogenic components may results in some information loss.

(iii) The performance of kernel combination consistently exceeds the one of score-level fusion. Under 100D feature space, the recognition rates for CKLR1 and CKLR2are 0.9661 and 0.9722, compared to 0.9487 for MAP,ofTG1, TG7, TG3,andTG9with the aspect view of 15°.

The first pair of targets(TG1andTG3) are armored personnel carriers, while the second pair of targets (TG2andTG4) are main-battle tanks. The results of four-target-recognition. The diagonal entries give the numbers of correct classified targets, while the others show the misclassified ones. The overall accuracies are in bracket.

0.9466 for SUM. The result corroborates that the classification via score-level fusion may be not effective the classes are not linearly separable.

(iv) The classification via summation kernel always exceeds the one via stacked features. Under 16D, 25D, 64D,and 100D feature spaces, the accuracies for CKLR2 are0.8942, 0.9271, 0.9681, and 0.9722, compared to 0.8901,0.9250, 0.9559, and 0.9661 for CKLR1.

3.1Comparison With the Conventional Methods

This subsection devotes to the comparison with the state-of the-art methods. Since the proposed methods are free-training, it is needed to choose the competitors likewise. Thus, k-NN,SVM, SRC MSRC , KSRC and KLR are employed as the baseline algorithms. Four targets, TG1, TG3, TG7,andTG9 are chosen from TABLE I. To assess the accuracies of individual class, the confusion matrices as well as the overall recognition rates are shown from which the following conclusions can be reached. First, it is more difficult to differentiate two main battle tanks (TG3 andTG9), whose scattering characteristics are very similar. For TG3, even 109 of 386 query samples are recognized asTG9 by k-NN, while the recognition rates obtained by MSRC, SRC, SUM, and MAP are 0.6736, 0.7668,0.6476, 0.6476, and 0.6606, much lower than the accuracies of remaining targets. This is because both configuration and depression are significantly different between the images used for training and those used for testing for TG1 and TG3.Second, the classifications in the Hilbert space always outperform the ones in the spatial domain. Compared the first row with the second row, we find the accuracy difference between two families of methods (classification in the spatial domain and the one in the Hilbert space) mainly comes from the recognition rate of TG3.ForTG3, the recognition rates obtained by KSVM, KSRC, KLR, CKLR1, and CKLR2 are 0.7538, 0.9611, 0.9559, 0.9870, and 0.9689.

4 EXPECTED RESULT

The proposed classification framework is valid in the case of random noise corruption. The stronger the noise, the better the proposed method performs compared to the competitors. (v) The proposed method could improve the recognition accuracy, especially under the extended operating conditions, e.g., structural modifications, variations in depression angle. The excellent performance shown by classification on the monogenic scale-space is the direct result of coupling the monogenic signal with sparse signal modeling. Thus, an intriguing question for our future work is whether the monogenic signal and sparse representation techniques could be used to the other stages for ATR, i.e., target detection and discrimination. We believe that the full potential of the monogenic signal and sparse representation in target detection and discrimination is yet to be uncovered. Secondly, the features used in Section III-B are defined via uniformly down sampling, normalization, and concatenation of the Components of the monogenic signal at different scales. Then,1-norm minimization problem becomes computationally tractable. In the future, we will explore some other techniques to combine the multiple components, and improve the performance simultaneously. Thirdly, the kernel function used in Section III-C is a general function, Gaussian RBF parameterized by the width. To improve the performance further, more attention will be paid to the task-specific kernels.

4.1 Classification via Kernel Combination

Previously, three individual classifications are formed on the monogenic scale-space, and the results of which are combined by score-level fusion scheme. Though the performance can be improved, it may be not effective if the classes are not linear separable. To address this problem, a popular idea is to cast the samples into the Hilbert space whose dimension is high or even infinite. Then, the similarity between a pair of samples can be estimated in a sufficiently rich feature space (F).

Given a nonlinear mapping $\varphi(\cdot)$: Rm _→ F, by which the monogenic features (17) can be cast into the Hilbert space. Inspired by the preceding work [34], where the spatial and spectral information are combined by constructing a family of composite kernels, this paper proposes to combine the information contained in the monogenic signal by composite kernel learning. We first integrate three component-specific Hilbert spaces into a larger global space, in which the similarity between a pair of samples could be evaluated more accurately. The proposed method can be summarized as

three sequential steps, as pictorially shown in Fig.4.

• Monogenic representation. For any new test sample **y**, it is represented by three monogenic feature descriptors, $\chi R(\mathbf{y})$, $\chi I(\mathbf{y})$, $\chi J(\mathbf{y})$, formed on log-Gabor filters induced monogenic scale-space.

• Kernel combination. The monogenic features are embedded into the Hilbert spaces with the nonlinear mappings. By stacked features or summation kernel, the component-specific Hilbert spaces are combined to form a larger global space.

• Make decision. In the global Hilbert space, the query is represented as a linear combination of training samples. The unique representation is generated by linear coding strategy, and the decision is made according to the characteristics of the representation on reconstruction.

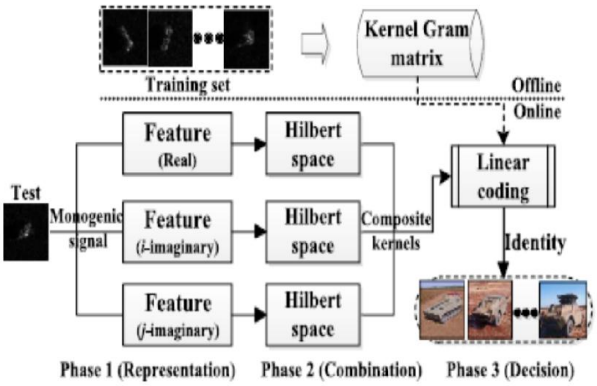

Figure 4.1: The flowchart of classification via kernel combination. The monogenic features generated on the monogenic scale-space are embedded into the Hilbert spaces. The component-specific Hilbert spaces are combined to form a larger one, in which linear coding strategy is used to make the decision.

Since the first step has been stated previously, the following section will pay more attention to kernel combination. In Section III-B, three monogenic features are generated on the monogenic scale-space. To combine the information contained in the monogenic features, this paper jointly considers these features into a unifying framework for target recognition. It is realized by a recently developed learning skill, kernel combination. Inspired by the preceding works [34], two schemes are contended.

5 EXPERIMENTS AND DISCUSSIONS

To verify the proposed method, extensive experiments are conducted on MSTAR database, a gallery collected using a 10 GHz SAR sensor in one-foot resolution spotlight mode. Images are captured at various depressions over a full 0 □ 359° range of aspect view. The depression refers to the angle between the line of the sight from the radar to the target and the horizontal plane at the radar. The chip images are of around 128×128 pixels in size, and cropped to 80×80 pixels region of interest. The number of aspect views available for these targets is listed in TABLE I, where the entries in parentheses are the series

number of variants with structural modifications, and the first row gives their generic labels. The three component-specific classifiers are notated as SRC*R*, SRC*I*, SRC*J* .
From TABLE III, some conclusions can be drawn.
(i) The classification via data fusion significantly outperforms the individual classifications. Under 16D feature space, the recognition rates for MSRC, SUM, and MAP are 0.8368, 0.8429, and 0.8542, compared to 0.6961 for SRC*R*, 0.7669 for SRC*I* , 0.8183 for SRC*J* .
The similar performance can be achieved under the other feature spaces.
(ii) The performance of score-level fusion always exceeds the one of feature-level fusion. Under 16D, 25D, 64D, and 100D feature spaces, the recognition rates for MAP are 0.8542, 0.8963, 0.9302, and 0.9487, compared to 0.8368, 0.8932, 0.9179, and 0.9322 for MSRC.
It is 1.74%, 0.31%, 1.23%, and 1.65% better than the competitor. The result proves that the combination by concatenating monogenic components may results in some information loss.
(iii) The performance of kernel combination consistently exceeds the one of score-level fusion. Under 100D feature space, the recognition rates for CKLR1 and CKLR2 are 0.9661 and 0.9722, compared to 0.9487 for MAP, Fig. 7. Examples of *TG*1, *TG*7, *TG*3, and *TG*9 with the aspect view of 15°.
The first pair of targets (*TG*1 and *TG*3) are armored personnel carriers, while the second pair of targets (*TG*2 and *TG*4) are main-battle tanks.
Fig. 8. The results of four-target-recognition. The diagonal entries give the numbers of correct classified targets, while the others show the misclassified ones. The overall accuracies are in bracket.
0.9466 for SUM. The result corroborates that the classification via score-level fusion may be not effective if the classes are not linearly separable.
(iv) The classification via summation kernel always exceeds the one via stacked features. Under 16D, 25D, 64D, and 100D feature spaces, the accuracies for CKLR2 are 0.8942, 0.9271, 0.9681, and 0.9722, compared to 0.8901, 0.9250, 0.9559, and 0.9661 for CKLR1.

5.1 Comparison With the Conventional Methods

This subsection devotes to the comparison with the state-of the-art methods. Since the proposed methods are free-training, it is needed to choose the competitors likewise. Thus, k-NN, SVM, SRC [18], [21], MSRC [23], KSRC [37], [38] and KLR [36] are employed as the baseline algorithms.
Four targets, *TG*1, *TG*3, *TG*7, and *TG*9 are chosen from TABLE I. Samples of the targets are shown in Fig. 7.
To assess the accuracies of individual class, the confusion matrices as well as the overall recognition rates are shown in Fig. 8, from which the following conclusions can be reached. First, it is more difficult to differentiate two main battle tanks (*TG*3 and *TG*9), whose scattering characteristics are very similar. For *TG*3, even 109 of 386 query samples are recognized as *TG*9 by k-NN, while the recognition rates obtained by MSRC, SRC, SUM, and MAP are 0.6736, 0.7668, 0.6476, 0.6476, and 0.6606, much lower than the accuracies of remaining targets. This is because both configuration and depression are significantly different between the images used for training and those used for testing for *TG*1 and *TG*3.
Second, the classifications in the Hilbert space always outperform the ones in the spatial domain. Compared the first row with the second row, we find the accuracy difference between two families of methods (classification in the spatial domain and the one in the Hilbert space) mainly comes from the recognition rate of *TG*3. For *TG*3, the recognition rates obtained by KSVM, KSRC, KLR, CKLR1, and CKLR2 are 0.7538, 0.9611, 0.9559, 0.9870, and 0.9689, compared to 0.6191 for kNN, 0.6476 for SRC, 0.6736 for MSRC, 0.6476 for SUM, and 0.6606 for MAP. The classifications via kernel combination achieve significant improvement in overall accuracy as well as individual recognition rate in comparison to the baseline methods. The results can be explained from the perspective of dataset.
Fig. 9. Illustration of random noise corruption. The set of images demonstrate that 0%, 5%, 10%, 15%, and 20% of pixels are corrupted.

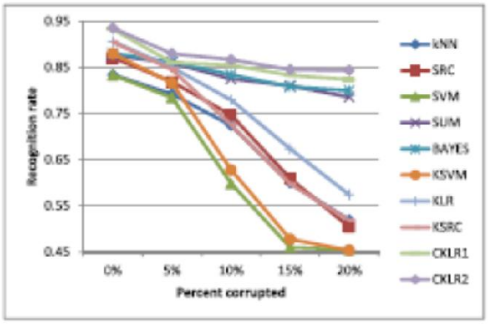

Figure 5.1: The recognition rate across the range of noise corruption.

Since the classes are not linearly separable, the prior assumption that samples of a certain class lie on a linear subspace is not founded. Fortunately, the shortage can be covered by embedding samples into the Hilbert space with a nonlinear mapping. Then, the similarities between a pair of samples can be measured in a sufficiently rich feature space. Last but not least, the monogenic signal representation, which is capable to capture the broad spectral information and simultaneous spatial localization with compact support, also contributes to the better performance.

5.2 Target Recognition Under Random Noise Corruption

For this experiment, we evaluate the performance of proposed methods in the case of strong noise. The experimental setup is similar to the one in Section IV-B. To simulate the noise, we corrupt a percentage of randomly chosen pixels from each of the query images, replacing their intensity with independent and identically distributed samples from a uniform distribution. The corrupted pixels are randomly chosen from the image, *i.e.*, the locations are randomly decided. We vary the percentage of corrupted pixels from 0 percent to 20 percent. A set of example images are given in Fig. 9.

Fig. 10 draws the recognition performance as a function of the level of noise corruption. The corresponding recognition rates are tabulated in TABLE IV. Here, the robust version of SRC, which solves the extended _1-norm minimization problem [18], is utilized to deal with the occlusion.

From Fig. 10 and TABLE IV, we could see that the performances are degraded with the range of corruption increased. From 0 percent upto 20 percent corruption, the recognition rates for MAP are 0.8804, 0.8602, 0.8339, 0.8082, and 0.7994, compared to 0.8708, 0.8186, 0.7464, 0.6091, and 0.5193 for the nearest competitor. A drop of 8.10% and 8.91% for recognition accuracy are obtained by MAP and SUM, compared to the drop of 37.81%, 36.68%, and 51.93% for SVM, SRC, and k-NN. The similar performances are obtained using two proposed kernel combination methods. At 20% corruption, none of the competitors achieves the recognition rate higher than 60%, while CKLR1 and CKLR2 achieve the recognition rate of 0.8234, and 0.8435. CKLR1 and CKLR2 are 24.96% and 26.97% better than the nearest competitor.

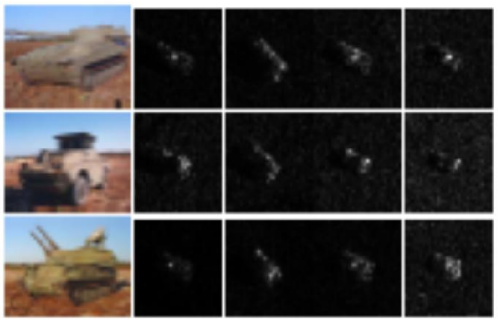

Figure 5.2: Example of three vehicle targets. The first, second, and third rows demonstrate SAR images of TG4, TG5, and TG6 collected at 15°, 17°, 30° and 45° depression.

From 0 percent to 20 percent, CKLR2 generates a drop of 9.14% for recognition rate, compared to the drop of 42.60%, 38.60%, 33.23% for accuracy by KSVM, KSRC, and KLR. The experimental results

prove that the proposed methods are valid in the case of strong noise. The stronger the noise, the better the proposed methods perform than the competitors.

Fig. 13. The performance under EOC difference on depression. In each sub-table, the row shows the ground-truth of the query sample, while the column displays the class membership predicted by the algorithms to be studied. The diagonal entries demonstrate the recognition rate of each class, while the non-diagonal entries represent the misclassification rate. The entries in parentheses are the overall recognition rates.

Figure 5.3: Examples of ten vehicle targets. Images of TG1, TG2, TG3, TG4, TG5, TG6, TG7, TG8, TG9, and TG10 with an aspect view of 40° are listed from left to right.

5.3 Target Recognition Under Depression Variations

This subsection considers target recognition under different depressions. Three similar targets, *TG*4, *TG*5, and *TG*6 are chosen from TABLE I, among which *TG*5 and *TG*6 have the articulated variants. The articulated refers to a physical change such as open hatch or rotated gun turret. An example of *TG*6 and the articulated variants are shown in Fig. 11. Images taken at 17° depression are used to train the algorithms, while the ones captured at 15°, 30°, and 45° are used for testing. The number of aspect views available for three targets at different depressions are listed in TABLE V, where the entries in parentheses denote the articulated variants.

Fig. 13 tabulates the overall recognition rates (in parentheses), as well as the confusion matrices obtained using various methods. The first scenario deals with a minor EOC difference on depression. It adheres to the standards set forth to train the algorithms at an operating condition of 17° depression and test them at an operating condition of 15° depression, *i.e.*, a change of 2° from 17° to 15° exists between the images used for training and those used for testing. As can be seen, all of the algorithms produce a satisfied result. The overall recognition rates for SRC, KSRC, KLR, MSRC, SUM, MAP, CKLR1, and CKLR2 are 0.9818, 0.9903, 0.9866, 0.9964, 0.9988, 0.9988, 0.9963, and 0.9975.

Two score-level fusion methods, SUM and MAP, even correctly recognize 821 of 822 query samples. The second scenario evaluates a medium EOC difference on depression. The algorithms are tested at an operating condition of 30° depression, *i.e.*, there is a change of 13° from 17° to 30° between the training samples and query samples.

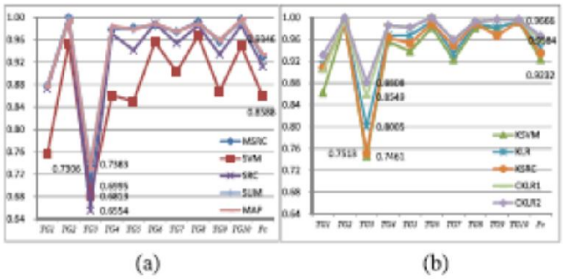

Figure 5.4:. The recognition rates with respect to the individual target class. Pc denotes the overall recognition rate; (a) and (b) plots the recognition rates obtained using the classifications in the spatial domain and the ones in the Hilbert space.

The performance is slightly degraded. The overall recognition rates obtained by SRC, KSRC, KLR, MSRC, SUM, MAP, CKLR1, and CKLR2 are 2.04%, 1.81%, 1.80%, 1.35%, 3.30%, 2.66%, 2.51%, and 1.46% lower than the rates at 15° depression. CKLR2 and MSRC produce the best performance, 0.9829. The third scenario considers a major EOC difference on depression. The algorithms are further tested at an operating condition of 45° depression, *i.e.*, a drastic change of 28° from 17° to 45°

exists between the training samples and testing samples. Obviously, the performance is sharply degraded. Two targets, *TG*4 and *TG*5 are easily to be confused due to the abrupt change in the signatures of the same target from different depression angles. The overall recognition rate for KSRC even declines by 42.78% and 44.59% compared to the ones at 15° and 30° depressions. However, the classifications via score-level fusion still achieve the overall recognition rates of 0.7186 and 0.7221, compared to 0.6394 for MSRC, 0.5453 for KLR, 0.5444 for KSRC, and 0.5366 for SRC. CKLR2 achieves the best recognition rate, 0.7456. It is 10.62%, 20.03%, 20.12%, and 20.90% better than MSRC, KLR, KSRC, and SRC.

From the experimental results, we come the following conclusions. The proposed method achieves the performance similar to the baseline algorithms under minor and medium EOC difference on depression (or standard operating condition). However, when the major EOC difference on depression is considered, it demonstrates better advantage than the reference methods. On the other hand, the results also prove that the tolerance towards variation in depression could be improved with the monogenic signal representation.

6 TARGET RECOGNITION

6.1 Image Load

The satellite image is given as input for target detection. The image can be of any standard sizes, such as 256×256, 1024×1024. Here the image with pixels 256×256 is considered and it is shown below.

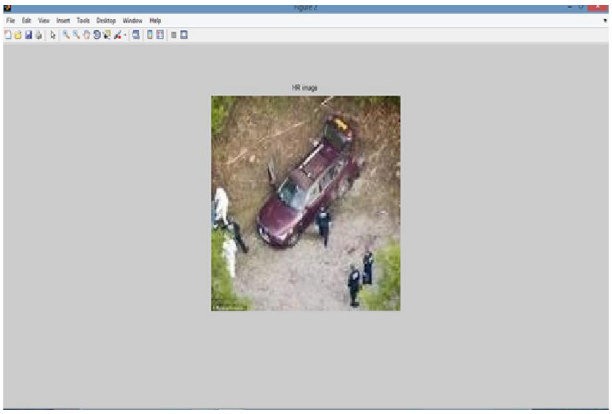

Figure 6.1*: *Input image

6.2 Image Filter

The input image is filtered using the Bayer filter. It is a color filter array and hence can record primary colors in an color image. The Bayer filter includes the bilinear interpolation. The filter can perform the operation such as noise removal, zooming, shrinking, sharpening, blurring, etc., and the filtered image is shown below.

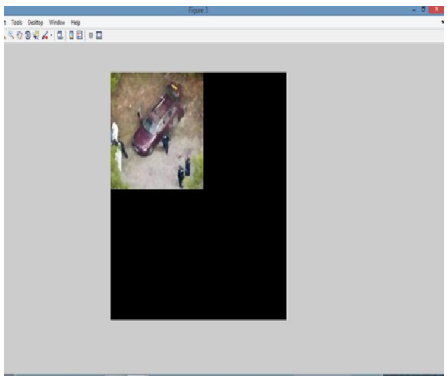

Figure 6.2*: *Filtered image

6.3 Image Segmentation

The filtered image is then segmented by using the Linear Discriminant Analysis. Segmentation involves the partitioning of the image in to small fragments of equal sizes.

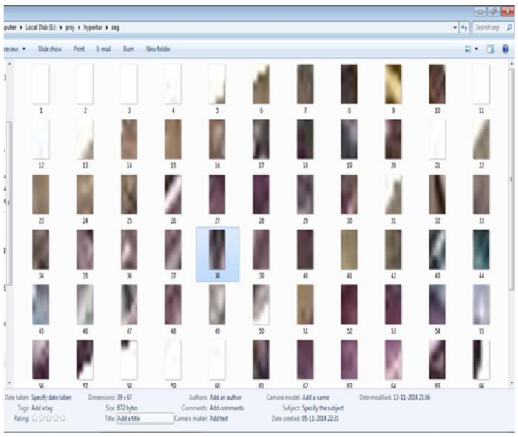

Figure 6.3*: *Segmented image

6.4 K-Mean

A segment is to be selected for the target detection. The algorithm will search for pixels which almost match the selected images pixel value.

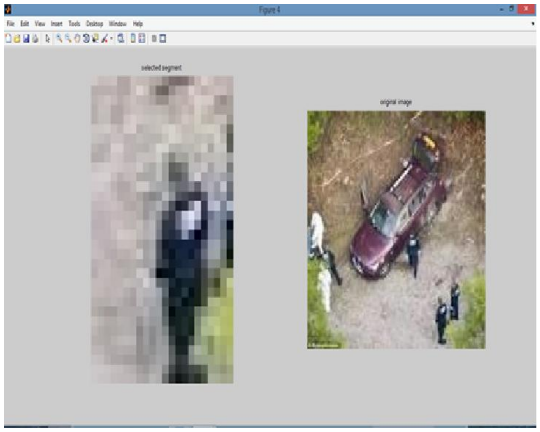

Figure 6.4*: *Selected segment

6.5 Feature Extraction

For target detection, the feature is to be extracted using the K-Means algorithm, and it is shown below.

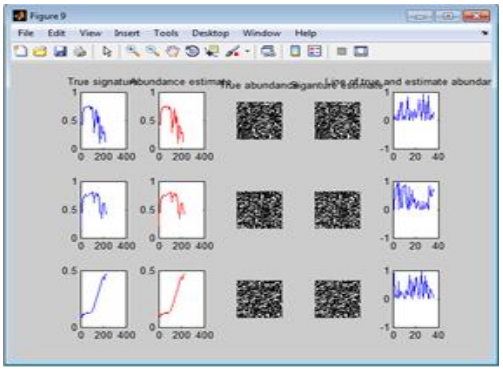

Figure 6.5*: *Feature extraction

6.6 Feature Extraction (Datapoints)

The three pixel values are considered such as the value of the target spectrum, unlabeled spectrum and background spectrum, and the data points are extracted by using this value, which can be calculated using the equation. The extracted data points showing true and estimated points are shown below.

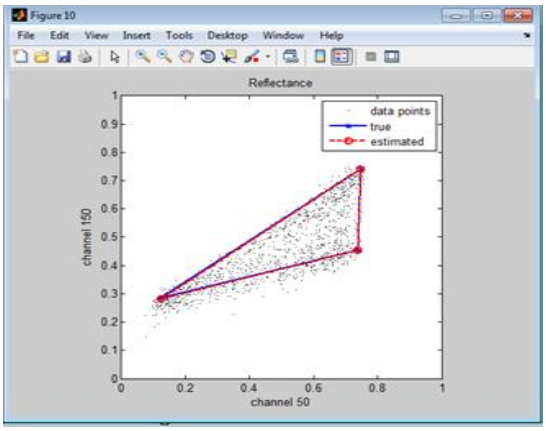

Figure 6.6*: *Feature extracted data points

6.7 Feature Extraction (Projected Data Points)

In K-Means, to maintain the dominant structure of the distribution after DR, we use the subspace arrived at by principal component analysis (PCA), based on the full input data matrix, to restrict the feature space learned by discriminative manifold embedding, which is only based on the given labeled data.
The points are to be projected, by using the data obtained in the input image and the image to be targeted. Hence the projected points are shown below.

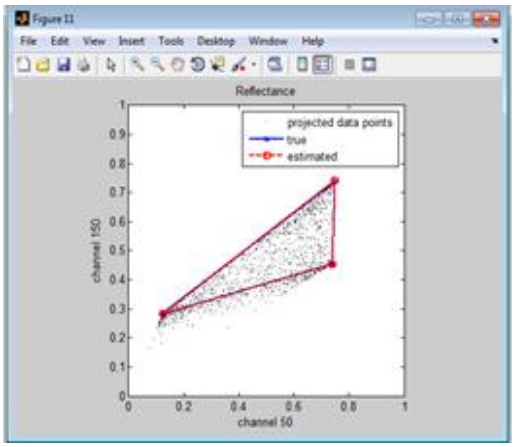

Figure 6.7*: *Feature extracted projected data points

6.8 Target Detection

Finally, the target detection result is obtained by sorting the nearest neighbors (NN) of the target feature vector in the sparse transfer manifold embedded feature space.

Hence the target is detected and hence the output image is obtained as shown below.

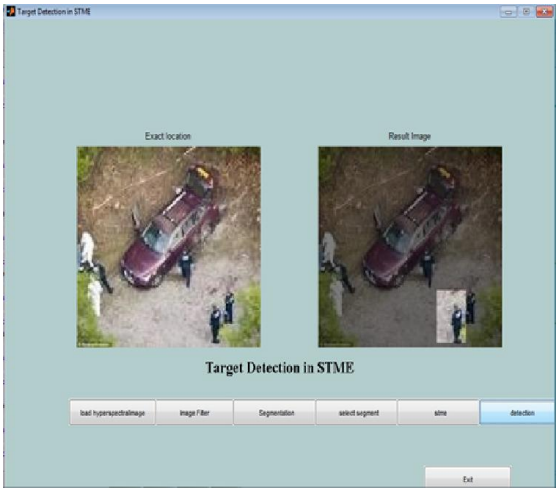

Figure 6.8*: *Output image

7 CONCLUSION

In this paper, we introduce a novel classification framework on the monogenic scale-space for target recognition in SAR image. The proposed method applies multiple linear regression models to the features derived from the components of the monogenic signal at different scales, and reaches the inference by evaluating which class of samples could recover the query as accurately as possible. It is robust towards EOC difference on depression and configuration, as well as noise corruption. The feasibility of the proposed framework has been successfully tested on MSTAR database, which is a standard testbed for SAR image interpretation. From the experimental results on MSTAR database, we draw the following conclusions: **(i)** The monogenic signal could effectively capture the characteristics of SAR image, *e.g.*, broad spectral information and simultaneous spatial localization, with compact support, and hence produce the excellent performance for target recognition. **(ii)** The classification via score-level fusion could combine the benefits of individual classification while tackling their drawbacks. Thus, the significant improvement in accuracy can be obtained. **(iii)** The classification via kernel combination could deal with the dataset whose target classes are not linearly separable, and hence improve the recognition accuracy. **(iv)** The proposed classification framework is valid in the case of random noise corruption. The stronger the noise, the better the proposed method performs compared to the competitors. **(v)** The proposed method could improve the recognition accuracy, especially under the extended operating conditions, *e.g.*, structural modifications, variations in depression angle.

The excellent performance shown by classification on the monogenic scale-space is the direct result of coupling the monogenic signal with sparse signal modeling. Thus, an intriguing question for our future work is whether the monogenic signal and sparse representation techniques could be used to the other stages for ATR, *i.e.*, target detection and discrimination. We believe that the full potential of the monogenic signal and sparse representation in target detection and discrimination is yet to be uncovered. To improve the performance further, more attention will be paid to the task-specific kernels.

REFERENCES

[1] E. R. Keydel, S. W. Lee, and J. T. Moore, "MSTAR extended operating conditions: A tutorial," *Proc. SPIE*, vol. 2757, pp. 228–242, Jun. 1996.

[2] T. D. Ross, S. W. Worrell, V. J. Velten, J. C. Mossing, and M. L. Bryant, "Standard SAR ATR evaluation experiments using the MSTAR public release data set," *Proc. SPIE*, vol. 3370, pp. 566–573, Apr. 1998.

[3] D. E. Dudgeon and R. T. Lacoss, "An overview of automatic target recognition," *Lincoln Lab. J.*, vol. 6, no. 1, pp. 3–9, 1993.

[4] L. M. Novak, G. J. Owirka, and C. M. Netishen, "Performance of a high-resolution polarimetric SAR automatic target recognition system," *Lincoln Lab. J.*, vol. 6, no. 1, pp. 11–23, 1993.

[5] Z. Jianxiong, S. Zhiguang, C. Xiao, and F. Qiang, "Automatic target recognition of SAR images based on global scattering center model," *IEEE Trans. Geosci. Remote Sens.*, vol. 49, no. 10, pp. 3713–3729, Oct. 2011.

[6] G. J. Owirka, S. M. Verbout, and L. M. Novak, "Template-based SAR ATR performance using different image enhancement techniques," *Proc. SPIE*, vol. 3721, pp. 302–319, Aug. 1999.
[7] R. Singh and B. V. Kumar, "Performance of the extended maximum average correlation height filter and the polynomial distance classifier correlation filter for multiclass SAR detection and classification," *Proc. SPIE*, vol. 4727, p. 265, Aug. 2002.
[8] D. Casasent and A. Nehemiah, "Confuser rejection performance of EMACH filters for MSTAR ATR," *Proc. SPIE*, vol. 6245, p. 62450D, Apr. 2006.
[9] K. Copsey and A. Webb, "Bayesian gamma mixture model approach to radar target recognition," *IEEE Trans. Aerosp. Electron. Syst.*, vol. 39, no. 4, pp. 1201–1217, Oct. 2003.
[10] M. D. DeVore and J. A. O'Sullivan, "Quantitative statistical assessment of conditional models for synthetic aperture radar," *IEEE Trans. Image Process.*, vol. 13, no. 2, pp. 113–125, Feb. 2004.
[11] J. A. O'Sullivan, M. D. DeVore, V. Kedia, and M. I. Miller, "SAR ATR performance using a conditionally Gaussian model," *IEEE Trans. Aerosp. Electron. Syst.*, vol. 37, no. 1, pp. 91–108, Jan. 2001.. 12, no. 6, pp. 1247–1251, Jun. 2015.